Computer Physics Communications 228 (2018) 30–37

Contents lists available at ScienceDirect

Computer Physics Communications

journal homepage: www.elsevier.com/locate/cpc

Stochastic analysis of surface roughness models in quantum wires

Mihail Nedjalkov [a], Paul Ellinghaus [a], Josef Weinbub [b,*], Toufik Sadi [c,e], Asen Asenov [c], Ivan Dimov [d], Siegfried Selberherr [a]

[a] Institute for Microelectronics, TU Wien, Gußhausstraße 27-29/E360, 1040 Wien, Austria
[b] Christian Doppler Laboratory for High Performance TCAD, Institute for Microelectronics, TU Wien, Gußhausstraße 27-29/E360, 1040 Wien, Austria
[c] School of Engineering, University of Glasgow, Glasgow G12 8LT, Scotland, UK
[d] Institute for Information and Communication Technologies, Bulgarian Academy of Sciences, Acad. G. Bonchev St., Block 25A, 1113 Sofia, Bulgaria
[e] Department of Neuroscience and Biomedical Engineering, Aalto University, P.O. Box 12200, 00076 AALTO, Finland

ARTICLE INFO

Article history:
Received 30 August 2017
Received in revised form 22 January 2018
Accepted 12 March 2018
Available online 21 March 2018

Keywords:
Wigner transport model
Quantum wire
Surface roughness
Signed particles
Electron state dynamics

ABSTRACT

We present a signed particle computational approach for the Wigner transport model and use it to analyze the electron state dynamics in quantum wires focusing on the effect of surface roughness. Usually surface roughness is considered as a scattering model, accounted for by the Fermi Golden Rule, which relies on approximations like statistical averaging and in the case of quantum wires incorporates quantum corrections based on the mode space approach.

We provide a novel computational approach to enable physical analysis of these assumptions in terms of phase space and particles. Utilized is the signed particles model of Wigner evolution, which, besides providing a full quantum description of the electron dynamics, enables intuitive insights into the processes of tunneling, which govern the physical evolution.

It is shown that the basic assumptions of the quantum-corrected scattering model correspond to the quantum behavior of the electron system. Of particular importance is the distribution of the density: Due to the quantum confinement, electrons are kept away from the walls, which is in contrast to the classical scattering model. Further quantum effects are retardation of the electron dynamics and quantum reflection. Far from equilibrium the assumption of homogeneous conditions along the wire breaks even in the case of ideal wire walls.

1. Introduction

Quantum mechanics progressively captures the physics of modern electronic nanostructures, designed around the concept of spatial confinement, where electrons are not any more point-like particles. Processes related to the superposition property, such as coherence and entanglement, provide a foundation for novel engineering disciplines, such as entangletronics [1], while the finite electron size introduces the need to take the Heisenberg principle into account for the proper description of the transport processes. Indeed, the momentum component of the electron in the direction of confinement is not any more a well-determined physical quantity. This requires to reconsider the models of the transport theory derived for a bulk crystal and in particular the mechanisms for electron interaction with the variety of deviations from the periodicity of the ideal crystal structure, ranging from atom vibrations to effects introduced by interfaces and edges.

Especially important for the behavior of nanoscale structures is the interface responsible for the confinement in one or more spatial directions , such as in quantum wires (also frequently referred to as nanowires). Already phenomenological considerations prompt that the properties of such interfaces should affect the evolution of the electron system in the structure. Surface roughness (SR) should impede the evolution of the electron system, compared to ideal surfaces. Theoretical and experimental studies show that SR is a dominant low-field electron mobility limiting mechanism in confined structures [2]. Models for both, pure bulk and confined structures, usually treat the electron–SR interaction as a scattering process, causing an instantaneous change of the electron momentum component (which is local in space) in the direction of transport: Namely, the usual models assume a decomposition of the problem into an eigenvalue task due to confinement and a transport task along the unconfined direction(s), where the electron momentum is well defined [3].

Electron evolution processes in quantum wires incorporate a major part of the transport phenomena governing the operation of actual nanoelectronic devices like FinFETs and quantum wire transistors [2–4]. In such structures the transport is along the wire.

* Corresponding author.
E-mail address: josef.weinbub@tuwien.ac.at (J. Weinbub).

https://doi.org/10.1016/j.cpc.2018.03.010
0010-4655/

The transverse confinement gives rise to an eigenvalue problem posed in terms of eigenfunctions and energy subbands. Within this approach shape variations are treated as perturbations. Scattering probability models based on the Fermi Golden Rule depend explicitly on the transverse eigenfunctions, while the subband energies appear in the energy conserving delta function. The latter captures the electron dynamics in the long-time limit of the electron-surface potential interaction process. The eigenvalue problem can be solved either for an ideal wire or with account for the rough interface [5]. Statistical averaging is performed, which gives rise to a model that is roughness-aware, and can be considered independent of the position along the wire.

In Section 2, we present the main assumptions and approximations inherent to this approach. The goal of this work is to use first principle quantum descriptions to analyze the physical effects caused by SR, and then draw a comparison with the assumptions inherent for a scattering model approach. The evolution of Wigner states [6] corresponding to minimum uncertainty wave packets, which are periodically injected through the source end of the simulation domain, are simulated in the cases of ideal or rough two-dimensional wire surfaces.

Of central importance is Section 3, which presents the numerical aspects of the utilized signed particles, computational model. The derivation of the latter is based on stochastic weights [7] obtained by applying the numerical Monte Carlo theory to an integral formulation of the Wigner transport problem. It has been shown that stochastic weights give rise to particles carrying positive or negative signs [8]. In the stationary transport case the corresponding numerical algorithm has been called pair-generation method [9]. The approach has been generalized recently for evolution problems and has been termed signed particle method. It has been shown that the continuous particle acceleration – according to Newton's second law – can be reproduced by the generation/annihilation of unaccelerated signed particles [10]: This may be considered as a major validation of the method, which provides a transition from a force to a potential description of the electron dynamics. Furthermore, signed particle attributes provide not only a simulation approach, but a particle picture, which can be regarded as an alternative formulation of Wigner phase space quantum mechanics. The model offers a high level of intuition and offers a profound apparatus for physical analysis.

Simulation results of the most important physical characteristics of semiconductor devices, namely the electron density and the current, along with an analysis of their evolution is presented in Section 4. Section 5 discusses certain computational aspects.

In summary, this manuscript makes the following three core contributions:

(1) Analysis of the physical factors which make the quantum-corrected SR scattering model a relevant replacement for the standard scattering model widely used in classical device simulators;

(2) Novel two-dimensional signed particles, simulation approach based on injection of coherent states from the boundary;

(3) An advanced view of the signed particle approach as a set of concepts which may be combined into different methods suitable for both stationary and transient physical problems in the presence of initial and/or boundary conditions.

2. Surface roughness scattering model

The Fermi Golden Rule, obtained within the time-dependent perturbation approach is the basic theoretical notion, giving the probability S for a transition *per unit time* from an initial state $|\mathbf{k}\rangle$ defined by quantum numbers $\mathbf{k}$ and energy $E_{\mathbf{k}}$, to a state $\mathbf{k}'$ under the action of a perturbing Hamiltonian H':

$$S(\mathbf{k},\mathbf{k}') = \frac{2\pi}{\hbar}\left|\langle\mathbf{k}'|H'|\mathbf{k}\rangle\right|^2\delta(E_{\mathbf{k}'} - E_{\mathbf{k}} \pm \hbar\omega) \tag{1}$$

Here the δ function is a result of a long time limit of the action of H' and ω is the frequency (if any) of the perturbation. This limit introduces the first essential assumption for a completed collision, which furthermore poses certain requirements about the energy and time scales of the electron evolution [11], which characterize, e.g., the Boltzmann transport model.

To obtain the matrix element $\langle\mathbf{k}'|H'|\mathbf{k}\rangle$, we need the electron states in the wire and the perturbing Hamiltonian H' corresponding to the SR type of scattering. For convenience, we consider a two-dimensional wire with a length L, a transport direction along y, and a direction of confinement in x. The eigenfunction set is secondly assumed to be:

$$\langle x, y|l, k\rangle = \xi_l(x)\frac{e^{iky}}{\sqrt{L}}; \qquad E_{l,k} = \epsilon(k) + E_l\,, \tag{2}$$

where $\epsilon(k) = \frac{\hbar^2k^2}{2m}$ is the kinetic energy of the electron, E_l is the energy corresponding to the eigensolution $\xi_l(x)$ of the Schrödinger equation defined by the potential V, determined by the transverse properties of the wire. In the ideal case the potential $V = V_0$ is zero inside the wire, between points $x = a$ and $x = b$, defining the wire width, and $V_0(a, y)$ and $V_0(b, y)$ are straight lines. SR is defined by the stretch $\Delta(y)$, along x, so that the potential becomes $V_0(x+\Delta, y)$ The perturbation H' is then given by

$$V_0 + H' = V_0 + \frac{\partial V_0(x)}{\partial x}\Delta = V_0 + eE(x)\Delta\,, \tag{3}$$

which may be justified by a heuristic, 'linear response' consideration: The perturbation of the energy is proportional to the force eE pressing the electron to the interface, and the deviation from the ideal shape.

The state representation (2) prompts that the electron states correspond to the ideal case where the potential does not dependent on y. This basic, second assumption for the mode space approach allows to decompose the problem into transport and confinement tasks.

Furthermore, it is important to note the character (which is local in space) of the third assumption given by (3), where the potential variation is replaced by its unperturbed derivative.

The dependence on y enters the perturbation via the offset Δ, however, it will be further averaged by taking the stochastic nature of the random function Δ into account. The statistically averaged square of the matrix element can be expressed after some calculations by the autocorrelation function $\overline{\Delta(y)\Delta(y')}$.

$$\overline{|\langle l', k'|H'|l, k\rangle|^2} = e^2|N(l, l')|^2\int\frac{dy}{L}\int\frac{dy'}{L}\overline{\Delta(y)\Delta(y')}e^{i(k-k')(y-y')} \tag{4}$$

with

$$N(l, l') = \int dx\xi^*_{l'}(x)E(x)\xi_l(x)\,. \tag{5}$$

This result depends on the distribution of the random function Δ. We assume that the autocorrelation function can be decomposed into a component slowly depending on the position y, and a component that drops rapidly with the distance $|y - y'|$.

$$\overline{\Delta(z)\Delta(z')} = D^2(z)R(|z - z'|) = D^2(z)e^{-\sqrt{2}|z-z'|/\lambda} \tag{6}$$

We use D^2 to indicate that the autocorrelation becomes the variance for $y = y'$. The last equality introduces the fourth assumption about the shape of R [12]. This leads to the final expression of the averaged matrix element:

$$\overline{|\langle l', k'|H'|l, k\rangle|^2} = e^2|N(l, l')|^2\mathcal{D}^2\frac{1}{L}\frac{2\sqrt{2}\lambda}{\left(2 + \lambda^2q^2\right)};$$
$$\mathcal{D}^2 = \int\frac{dy}{L}D^2(y)\,, \tag{7}$$

where the mean offset, $\mathcal{D}$, is the averaged variance along the wire. The autocorrelation function has been effectively averaged to

$$\overline{\Delta(y)\Delta(y')} = \mathcal{D}^2 e^{-\sqrt{2}|y|/\lambda}\,. \tag{8}$$

In this way SR effects are captured by the two parameters $\mathcal{D}$ and λ which do not depend on y. They are usually determined by the methods of reverse engineering, e.g., by a comparison of experimental and simulation results.

The above assumptions are critical: They allow to consider the interaction of the electron with the wire surface as a stochastic process of scattering, described by a model similar to the models used in the case of impurity or phonon scattering.

We end up with the conclusion that the efforts to account for SR effects, which characterize inhomogeneous wires, lead to an entirely homogeneous model, where all involved physical processes are described by two statistical parameters. It is thus noteworthy to have a more detailed picture of the underlying physics related to these assumptions. Thus our goal is not to explore the engineering and application aspects of the above model, which is actually widely used in device simulations. Indeed, the model can be plugged into different approaches based on Boltzmann, Wigner, or Non-Equilibrium Green's Functions. However, a comparative study of surface roughness-aware transport approaches is beyond the scope of this work. Here, our goal is to obtain a deeper understanding of the underlying physical processes which make the model a feasible add-on to first principle quantum simulations. In a first principles treatment surface roughness is part of the boundary conditions. Thus, the above assumptions are explored here by using a Wigner particle picture in the case of a concrete surface, randomly generated by using typical values for the two parameters. This surface represents one of the many possible samples accounted for in the average given by Eq. (8).

The associated signed particle picture of the Wigner theory does not only lead to numerical methods for stochastic simulation, but also to heuristic models for physical analysis in terms of particles and phase space. It has been shown that the signed particle picture provides an independent formulation of quantum mechanics [13] and has been applied to simulations of a variety of physical problems including many-body systems [14] and density functional theory [15].

The concept of signed particles and the numerical aspects of their application to the SR aware transport problem are discussed in the next section.

3. Wigner signed particles

We present the main ideas giving rise to different models and algorithms which have the concept of signed particles in common. Theoretical studies about the possibility to develop particle approaches for the Wigner equation were developed in the past [16] and were first implemented for a stationary transport problem [17]. The core idea is to apply the numerical theory of the MC method for solving integral equations to different integral forms of the transport equation. Our presentation follows the historical evolution of the concepts, which offers a rather heuristic way to introduce the attributes of the signed particles. The development of these attributes has begun already 15 years ago for the stationary transport problem, defined by boundary conditions: This problem is especially focused on this section, in order to show that there is not a single, unique signed particle model, but rather a set of attributes which may be combined into a variety of algorithms suitable for particular tasks. It is then shown how these concepts can be modified and completed, as it has been recently done for the transient task of evolution from an initial condition [10].

In the next section, we first summarize the numerical aspects.

3.1. Numerical aspects

Let us consider a Fredholm integral equation of a second kind, with a kernel K and a free term f_0:

$$f(Q) = \int dQ' f(Q')K(Q', Q) + f_0(Q)$$

$Q \in \Omega$, Ω is domain from R^n, called simulation domain and $K \in L_2(\Omega \times \Omega), f_0 \in L_2(\Omega)$ are known functions [18]. The solution $f(Q)$ is given by the series

$$f(Q) = \sum_i f_i(Q); \quad f_i(Q) = \int dQ' f_{i-1}(Q')K(Q', Q) \tag{9}$$

obtained by the iterative replacement of the equation into itself. The convergence of the Neumann series (9) is analyzed in [19].

A multi-dimensional integral can be presented as the expectation value

$$f_i(Q) = \int dQ' P(Q, Q') \frac{f_{i-1}(Q')K(Q', Q)}{P(Q, Q')}$$

of the random variable given by the term in the fraction distributed by the term P, called transition probability for any fixed Q, which, except from some constrains, can be freely chosen. The expansion of this equation presents f_i as a product of probabilities P with the quantity $\frac{P}{K} \cdot \frac{P}{K} f_0(Q_i)$ called weight. The consecutive applications of P give rise to a numerical trajectory $Q, Q_1, \ldots, Q_i$. The trajectory links the initial point, where the solution is evaluated, with the point Q_i, where the contribution of f_0 is evaluated.

As applied to physical problems, where f plays the role of a distribution function and f_0 to the initial or boundary condition [20], the above fundamental algorithm is modified to compute mean values $\langle A \rangle$ given by the integral of f with generic physical quantities A, like electron density or velocity. In this case it is convenient to consider the adjoined equation with a solution

$$g(Q') = \int dQ K(Q', Q)g(Q) + A(Q')\,,$$

where A is assumed also from $L_2(Q)$. An important result is that physical averages can be expressed via g.

$$\langle A \rangle = \int dQ' A(Q')f(Q') = \int dQ f_0(Q)g(Q) = \sum_i \langle A \rangle_i \tag{10}$$

Now, by applying the fundamental algorithm, we obtain a trajectory which is constructed in the opposite direction: It begins from a point, where f_0 is evaluated and consists of consecutive points Q_i, which are used to evaluate the consecutive weights sampling the terms $\langle A \rangle_i$. The first point Q can be chosen by another probability p, called initial probability sampling the random variable $f(Q)/p(Q)$, which is the first term in the product giving the consecutive weights.

Finally the value of the physical average is obtained by the statistical mean of N trajectories giving N independent realizations of $\langle A \rangle$.

We conclude that in order to formulate a MC method it is sufficient to specify the transport equation in terms of variables, kernel, and free term, as well as the initial and transition probabilities. Our ambition is spread beyond the numerical aspects of the stochastic formalism: We intend, by choosing a proper set of probabilities P and p, to add a physical interpretation of the process of construction of the numerical trajectories. We begin with the simpler, stationary task.

3.2. Stationary transport particle attributes

In the stationary case the point Q corresponds to a multi-dimensional phase space point with coordinates $\mathbf{r}, \mathbf{k}$. The kernel is [17]:

$$K(\mathbf{r}', \mathbf{k}', \mathbf{r}, \mathbf{k}) = \int_{-\infty}^{0} dt' \Gamma(\mathbf{r}', \mathbf{k}', \mathbf{k}) e^{-\int_{t'}^{0} \gamma(\mathbf{r}(y))dy} \delta(\mathbf{r}' - \mathbf{r}(t')) \theta_D(\mathbf{r}') \tag{11}$$

where the fieldless Newtonian trajectory $\mathbf{r}(t') = \mathbf{r} + \frac{\hbar \mathbf{k}}{m} t'$ is initialized by $\mathbf{r}, \mathbf{k}$ at time 0, m is the effective mass, θ_D is the spatial indicator of the simulation domain,

$$\Gamma(\mathbf{r}, \mathbf{k}', \mathbf{k}) = V_w^+(\mathbf{r}, \mathbf{k}' - \mathbf{k}) - V_w^+(\mathbf{r}, \mathbf{k} - \mathbf{k}') + \gamma(\mathbf{k}) \delta(\mathbf{k} - \mathbf{k}') \tag{12}$$

$$V_w^+ = V_w \xi(V_w); \qquad \gamma(\mathbf{r}) = \int d\mathbf{k} V_w^+(\mathbf{r}, \mathbf{k}) \tag{13}$$

with ξ the Heaviside step function. Finally,

$$V_w(\mathbf{r}, \mathbf{k}) = \frac{1}{i\hbar(2\pi)^3} \int d\mathbf{s} e^{-i\mathbf{k}\cdot\mathbf{s}} \left(V(\mathbf{r} - \frac{\mathbf{s}}{2}) - V(\mathbf{r} + \frac{\mathbf{s}}{2}) \right) \tag{14}$$

is the Wigner potential, obtained from the electric potential V. The free term

$$f_0 = f_b(\mathbf{r}(t_b), \mathbf{k}(t_b)) e^{-\int_{t_b}^{0} \gamma(\mathbf{r}(y))dy} \tag{15}$$

which accounts for the boundary conditions f_b via the boundary time t_b - the value of the time for which $\mathbf{r}(t)$ becomes a boundary point. f_b appears to be the same as in the Boltzmann transport case [21], which is related to the fact that classical and Wigner-quantum equilibrium functions coincide.

A reformulation of the problem with the help of the adjoined equation offers several advantages: The numerical trajectories now begin from the boundaries, moreover the classical algorithm for injection of particles can be used for selection of the initial point. Second, the backward parametrization of the trajectory $\mathbf{r}(t'), t' < 0$ becomes a forward one, $t' > 0$. The terms in the series (10) are obtained by the iterative application of the following term:

$$\tilde{K}(\mathbf{r}', \mathbf{k}', \mathbf{k}, t) = e^{-\int_0^t \gamma(\mathbf{r}'(y))dy} \theta_D(\mathbf{r}'(t)) \Gamma(\mathbf{r}'(t), \mathbf{k}'(t), \mathbf{k}) . \tag{16}$$

The next step is to decompose (16) into conditional probabilities. By multiplying and dividing by γ it is obtained:

$$\tilde{K}(\mathbf{r}', \mathbf{k}', \mathbf{k}, t) = p_t(t, \mathbf{r}', \mathbf{k}') \theta_D(\mathbf{r}'(t)) \left\{ P_w^+ - P_w^- + P_\delta \right\} (\mathbf{r}'(t), \mathbf{k}', \mathbf{k}) 3 \tag{17}$$

with

$$p_t = \gamma(\mathbf{r}'(t)) e^{-\int_0^t \gamma(\mathbf{r}'(y))dy}; \tag{18}$$

$$P_w^{\pm}(\mathbf{r}'(t), \mathbf{k}', \mathbf{k}) = \frac{V_w^+(\mathbf{r}'(t), \pm(\mathbf{k}' - \mathbf{k}))}{\gamma(\mathbf{r}'(t))}; \quad P_\delta = (\mathbf{k}' - \mathbf{k}) . \tag{19}$$

These conditional probabilities can be used to construct the transition probability $P(\mathbf{r}', \mathbf{k}', \mathbf{k}, t)$ from point $\mathbf{r}', \mathbf{k}'$ to point $\mathbf{r} = \mathbf{r}'(t), \mathbf{k}$. p_t coincides with the Boltzmann probability for finding the next scattering time with the power of the Wigner potential γ playing the role of a scattering rate. This provides t and thus the spatial coordinate $\mathbf{r} = rv'(t)$ of the next phase space point. At this step the indicator θ_D kills the numerical trajectory, if $\mathbf{r}(t')$ is outside the simulation domain. Here we conclude that a trajectory begins by an event corresponding to a boundary injection of a classical particle and survives until evolving inside the simulation domain. In the latter case the wave vector coordinate $\mathbf{k}$ is generated by the probabilities enclosed in the curly brackets.

However, we first need to choose which of the terms to be the generator of the particular point. We have two options:

(a) To associate three probabilities ξ_i for choosing randomly which one continues the trajectory. In this case the successive iterations contribute to the weight by a factor P_i/ξ_i. For example, if $\xi_i = 1/3$, the total weight accumulated on a trajectory becomes a factor ± 3 with any new point added to the trajectory. Considering computational implementations, this, however, easily leads to a high memory demand, since the total weight grows exponentially with the simulation time. The approach works unfortunately only for electric potentials or simulation domains which are several orders of magnitude smaller than the values posed by realistic problems.

(b) The second option is to leave part of the weight in the phase space points, which can be used to initialize novel trajectories aiming to remove the residual weight. An important property which will be further exploited is that a weight with a given sign can cancel the same amount of weight with the opposite sign if stored at the same place.

Now the dilemma is what should be the next step after the numerical trajectory leaves the domain: (i) To begin a new one from the boundaries or (ii) to take care of the residual weight. The problem has been solved by an algorithm, where (i) and (ii) are alternating. The algorithm provides an unbiased estimator of the expectation value of interest [17].

The next step is to abandon the scattering comprehension of the terms in the curly brackets in favor of a generation comprehension: All three terms generate a value of $\mathbf{k}$ which leads to a maximal randomization of the weight. At this point we are ready to formulate the basic interpretation of the stochastic algorithm for construction of a numerical trajectory, which introduces the concept of particle sign:

1. The trajectory begins with a boundary injection of an initial particle at a point $\mathbf{r}', \mathbf{k}'$ ($\mathbf{r}'$ belongs to the boundary). The particle weight is set to unity.
2. A free flight over a Newtonian trajectory initialized by $\mathbf{r}', \mathbf{k}'$ at time 0 continues until time t selected according to a scattering rate given by γ, which determines $\mathbf{r} = \mathbf{r}'(t)$.
3. A generation of three wave vector values $\mathbf{k}_i$ follow ed, e.g., by the scheme: $\mathbf{k}_3 = \mathbf{k}'$, as determined by P_δ. Then $\mathbf{q}$ is generated according to $P_w^+(\mathbf{k}', \mathbf{q})$, so that $\mathbf{k}_2 = \mathbf{k}' - \mathbf{q}$ and $\mathbf{k}_3 = \mathbf{k}' + \mathbf{q}$.
4. The three phase space points $\mathbf{r}, \mathbf{k}_i$ become initial points for novel numerical trajectories in the next iteration step. The genuine particle survives and two novel ones are generated: Particle 2 retains the genuine weight, while particle 3 multiplies it by -1. The weights are taken into account in the computation of the physical averages of interest at any step of the iterative procedure.

This creates a picture of classical-like particles which are injected from the boundary with a positive sign and evolve over a Newtonian trajectory until leaving the simulation domain. According to rules determined by the Wigner potential they generate couples of secondary particles with $\pm$ sign, which, in turn, continue over their own Newtonian trajectories, generating ternary particles , and so forth. Positive and negative particles with a common phase space coordinates annihilate each other. Here it is important to note the role of the time integral in (11). After accounting for the delta functions, only a single time integration survives in the estimator of $\langle A \rangle$. It is, however, sufficient to ensure the ergodicity of the task and to replace the ensemble average over N trajectories (in the new *language*: N particles) by a time average. This means that a single particle is followed during the simulation. After leaving the simulation domain it is re-injected from the boundary or a point with a residual weight.

It is important to note that this picture is not unique. There are many options to modify the probabilities so that, e.g., a positive

or negative single particle is generated at a time. The advantage of the presented method is that the charge is strictly conserved as it generates particles pairwise with opposite sign. However, even this method is not unique [22].

3.3. Transient transport particle attributes — initial condition

In the transient case the time becomes an active variable and the point Q corresponds to a phase space — time point with coordinates $\mathbf{r}$, $\mathbf{k}$, t. The kernel is

$$K(\mathbf{r}', \mathbf{k}', t', \mathbf{r}, \mathbf{k}, t) = \Gamma(\mathbf{r}', \mathbf{k}, \mathbf{k}', t')e^{-\int_{t'}^{t}\gamma(\mathbf{r}(y),y)dy}\theta(t-t')\delta(\mathbf{r}'-\mathbf{r}(t'))\theta_D(\mathbf{r}'). \quad (20)$$

Integration variables are the primed ones, in particular the time integral is in the limits $0, \infty$. The free term f_0 involves the initial condition f_i which is defined via the Newtonian trajectory $\mathbf{r}(t')$ at time 0.

$$f_0 = f_i(\mathbf{r}(0), \mathbf{k})e^{-\int_0^t \gamma(\mathbf{r}(y),t)dy}; \quad \mathbf{r}(t') = \mathbf{r} + \frac{\hbar\mathbf{k}}{m}(t-t') \quad (21)$$

The functions Γ and γ now depend on time via the electric potential $V(\mathbf{r}, t)$. The general structure of the kernel resembles the stationary counterpart, in particular the models for free flight selection and the generation of particles remain the same. However, in this case, we can no more rely on the ergodicity of the system. The time averaging provided by a single trajectory is now replaced by an ensemble average. N particles are associated to the initial condition. Their evolution must be followed synchronously in time. The ensemble provides the physical averages at certain time fixed for all particles — initial and generated. As the number of the latter grows exponentially in time, the particle annihilation continues to be of crucial importance for reducing the computational burden. However, now annihilation is seriously hindered by the lack of ergodicity: It is no more sufficient for two particles with opposite sign to meet in the phase space in order to annihilate, they must have evolved to the same evolution time.

The problem has been solved due to the Markovian character of the evolution: At periodic time steps particles are recorded (i.e. summing the signs which results in annihilation) in phase space, which gives rise to a reduction of their number. To facilitate this process, a discrete momentum space has been introduced [23].

From a numerical point of view this considerably reduces the numerical error, since the iterative action of the kernel onto itself can be viewed as a forth and back Fourier transform. Discrete momentum is also motivated from a physical point of view: Physical systems like nanoelectronic structures are usually bounded by a maximal length where coherence exists. The momentum offset $\Delta\mathbf{k}$ is directly linked to the coherence length $\mathbf{L}_c$ by the relation $\Delta\mathbf{k} = \pi/\mathbf{L}_c$. In this way all spatial integrals are bounded by $\mathbf{L}_c$, while the momentum integration is replaced by a summation $\int d\mathbf{k} \to \sum_{m=-\infty}^{\infty} m\Delta\mathbf{k}$.

Now an important question arises: How can a discrete momentum space be compatible with Newtonian acceleration? This question has been addressed as a general test and verification of the particle sign concepts [10]. For convenience a one-dimensional problem is considered. The classical evolution of an initial peak $f(x, k, 0) = N\delta(k)\delta(x)$ corresponds to a continuous acceleration by E of the particles over a Newton trajectory. According to the quantum model, positive or negative particles are generated and annihilate each other on the discrete momentum space points with a spacing $\Delta k = \pi/L$.

Simulations show that this happens in such a way, that particles on the initial node gradually decrease in favor of an increase on the node to be occupied next. This results in a consecutive translation of the peak between the adjacent nodes. The instances Δt of full transfer between the nodes are consistent with Newton's law: $\hbar\Delta k = eE\Delta t$. Certain quantum effects are observed and associated to the discrete picture. The analysis shows that they disappear in the limit $\Delta k \to 0$ [10]. This is consistent with the fact that classical and quantum evolution are equivalent for linear potentials $V(x) = Ex$, which is expressed by the equality: $\int dk' V_w(k-k')f(x, k', t) = -eE\partial f(x, k, t)/\hbar\partial k$, obtained with the help of generalized functions and thus holds in the case $L \to \infty$. This establishes the transient signed particle concepts as an alternative to the continuous process of Newton acceleration, which it approaches asymptotically as the resolution of the discrete k-space increases.

3.4. Transient transport particle attributes — boundary conditions

We are finally ready to utilize the developed concepts of signed particles for constructing an algorithm appropriate for the SR simulation task. We compare the evolution of current and density in an ideal wire and a wire characterized by surface potential variations, as dependent on the periodic injection of electron states from the source contact.

This means that we have to use the evolution concepts from Section 3.3, while the approach to the boundary conditions must be adopted from Section 3.2. As discussed in Section 3.2, adjoined MC trajectories begin from the boundaries, where f_b, (15), is defined. Since f_b is zero outside, a transformation from a domain to a boundary integral is possible, which gives rise to a velocity weighted term $f_b|\mathbf{v}_b|$, where $\mathbf{v}_b(\mathbf{k}_b)$ is the normal component of the inward-directed velocity.

Within a formal stochastic approach $f_b|\mathbf{v}_b|$ must be used to construct a probability for the choice of the initial boundary point [17]. Here we use a peculiarity of the physical task, allowing to replace the boundary term by an initial term, which ensures indirectly the velocity-weighted boundary condition. We wish the trajectories initialized on the boundary to correspond to the process of injection of a minimum uncertainty Wigner state

$$\phi_w(\mathbf{r}, \mathbf{k}) = Ce^{\frac{-(\mathbf{r}-\mathbf{r}_0)^2}{\sigma^2}}e^{-(\mathbf{k}-\mathbf{k}_0)^2 2\sigma^2} \quad (22)$$

with C a normalization constant and σ is the variance, which for simplicity is assumed the same for both spatial directions x and y.

Now we assume a particle distribution initialized with the help of the two Gaussian functions in (22). The flux of such particles through any boundary initially placed outside the region of initialization is $f_b|\mathbf{v}_b|$ with f_b given by the value of ϕ_w on that boundary. Therefore any such particle obeys the distribution corresponding to the velocity-weighted boundary term and becomes a legitimate initial point of an adjoined MC trajectory in the moment of crossing the boundary.

We note that in contrast to Section 3.2 now f_b is a time-dependent function, determined by the distance between $\mathbf{r}_0$ and the boundary. Thus if we wish the injection to begin at time 0, the Wigner state must be detached to the boundary, which ensures that the first particles penetrate into the domain without a delay. This consideration must be taken into account especially in the case of consecutive injection of states with varying σ as required, e.g., in the case of equilibrium.

4. Simulation results and analysis

The aim of the presented simulations of electron transport in quantum wires is to analyze the physical processes as well as to evaluate the magnitude of certain characteristic quantities in conjunction with the four assumptions of the stochastic model (cf. Section 2). The Wigner particle approach ensures a first principles treatment of quantum transport, which directly challenges the last three assumptions of Section 2. Indeed, first the mode

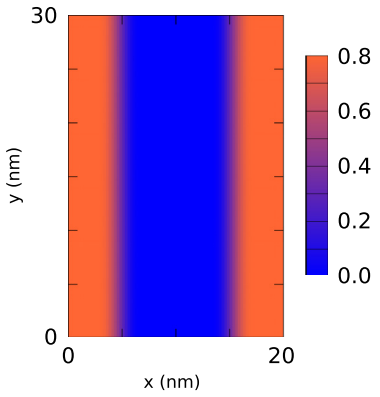

Fig. 1. The wire is defined by two 0.8 eV high and 5 nm wide walls, which smoothly drop to zero within a few nanometers towards the middle of the channel.

space representation of the electron state (2) is now given by the two-dimensional evolution of the Wigner equation solution. Furthermore, the local force in (3) is now replaced by the complete electric potential which determines the Wigner potential operator in the equation. Finally, the surface roughness must be considered as a part of the electrostatic boundary conditions, since stochastic processes cause irreversibility in the system evolution which contradicts the first principle origin of the description. A concrete surface is randomly generated by using typical values for the two parameters $\mathcal{D}$ and λ. As discussed earlier, such a surface represents one of the many possible counterparts accounted for in the average given by Eq. (8).

The above considerations concern also the typical equilibrium conditions commonly applied to semiconductor structures in the injecting contact. They need to be abandoned in favor of a coherent injection approach: The fundamental representation of a particle in the pure state Schrödinger mechanics is the minimum uncertainty wave packet. The corresponding Wigner pure state is given by function (22). Injection of states with a constant σ is a necessary condition for a coherent evolution: Indeed, injection of mixed states, e.g., according to Fermi–Dirac or Maxwell–Boltzmann distributions, already introduces decoherence in ballistic devices [24]. Thus, in the case of coherent injection, σ does not vary according to a given distribution, but is kept constant.

The aim is twofold: Firstly, to avoid smearing of the results due to the thermal averaging which helps to outline the quantum effects, and secondly, to allow the imposition of conditions far from equilibrium.

Based on our computational approach, we focus on the electron density, velocity, and current. We note the lack of dissipation processes: The total energy is conserved in the electron–potential interaction. In general, the chosen values of the physical quantities and parameters are typical for semiconductor electrons.

Fig. 1 shows the simulation domain and the potential profile. The ideal wire is defined by two 0.8 eV high, 5 nm wide walls, which smoothly drop to zero within a few nanometers towards the middle of the channel. Smoothing is necessary to avoid artificial frequencies which are otherwise introduced in the system by Fourier transforms of abrupt potential changes. A Tukey window is used for the smoothing, details are given in [25].

Equivalent Wigner states with $\sigma = 2$ nm, corresponding to the mean equilibrium electron energy at room temperature, are regularly injected through the $y = 0$ boundary of the wire with a period of 5 fs (Fig. 1).

They are initialized several σ below the point $x = 10, y = 0$: Fig. 2 shows the density after 50 fs evolution, which corresponds to the injection of 10 boundary states with central wave vector

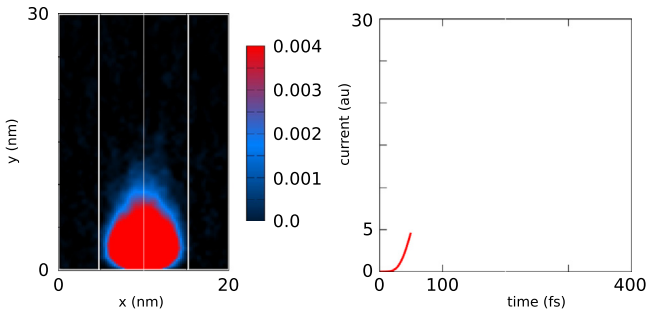

Fig. 2. Density (in arbitrary units) after injection of 10 states (left). The potential walls and the middle of the wire are denoted by white lines. The current just begins to increase, which outlines the transient regime of the evolution (right).

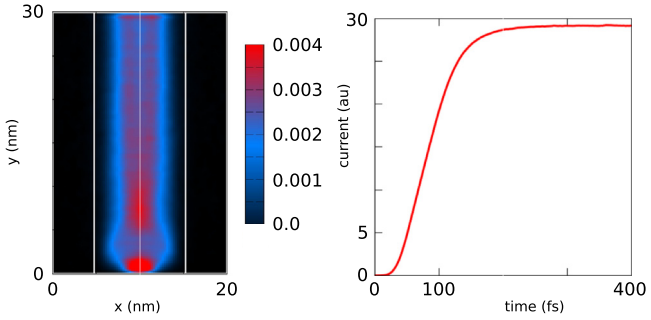

Fig. 3. Density (in arbitrary unit) after 400 fs evolution (left). The system enters into a stationary regime after 200 fs, as seen from the current which remains constant during the next 200 fs (right).

values of $k_{0x} = 0$, $k_{0y} = 7\Delta k$. The square mesh in the momentum space ($\Delta\mathbf{k} = \pi/\mathbf{L}_c$) is determined by a coherence length $\mathbf{L}_{c;x,y} = 45$ nm and corresponds to an energy of 1 meV for an effective mass of 0.19. With this choice of the coherence length all points of the simulation domain, but these belonging to the two 7.5 nm wide y-strips adjacent to the source and drain regions and left to decouple the injection from absorption regions, are correlated via the Fourier transform for the Wigner potential kernel. Since the electron density outside of the device domain is zero, the action of the Wigner kernel is restricted to the inside of the domain, so that a further augmentation of $\mathbf{L}_c$, besides the reduction of $\Delta\mathbf{k}$, has no physical effect. On the contrary, a reduction of $\mathbf{L}_c$ causes decoherence and transition to classical behavior: It can be shown that the effect of a stochastic scattering (e.g by phonons) causes an effective reduction of the coherence length [26].

We note that the governing physical process is tunneling, as there are no artificial boundaries to reflect the particles. Additionally, all particles leaving the simulation domain are absorbed, c.f. Section 3.

An initial spread towards the walls is clearly visible, until the potential redistributes the electron density along the channel. The current, calculated with the Ramo–Shockley theorem [27], linearly increases due to the periodic injection of electron states. After 200 fs, steady-state conditions are reached, as suggested by the behavior of the current in Fig. 3.

The initial spread of the density near the injecting contact remains until the quantum repulsion establishes control by squeezing the electron system away from the walls. One can easily create a reference picture with a classical evolution, where electrons are reflected only by a contact with the walls and thus are spread to the white lines marking the walls. Furthermore, the effect of the contacts is well pronounced, so that the density is homogeneous along the middle of the wire in y-direction. The abrupt change of the

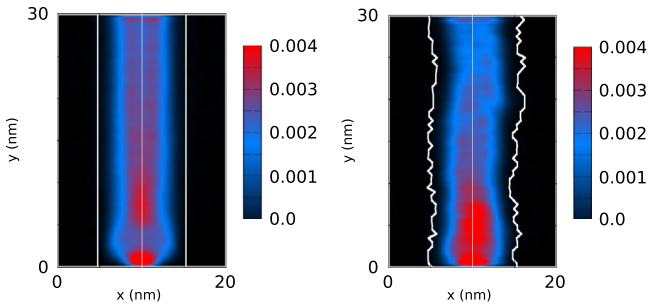

Fig. 4. Density (in arbitrary unit) after 400 fs evolution of the ideal (left) and the rough wire (right). Here $k_{0y} = 5\Delta k$, corresponding to an energy of 0.25 meV.

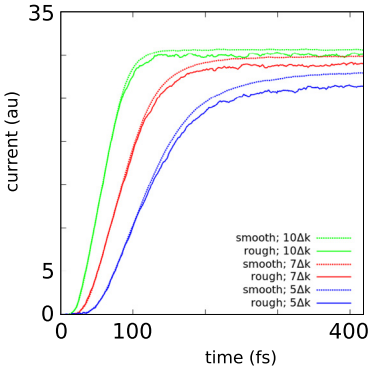

Fig. 5. Current evolution in the ideal and rough wires for three different values of k_{0y}, corresponding to kinetic energies of 100 meV, 50 meV, and 25 meV.

physical conditions near the injecting and the absorbing contacts modifies the electron distribution. The simulation provides useful information about the approximate length scale where the density may be considered as piecewise homogeneous. The effect depends on the boundary conditions and should vanish near equilibrium, as expected from physical considerations.

The assumptions related to the mode space approach are expected to be seriously challenged in the case of a rough surface. The latter is obtained by superimposing variations of the potential with the autocorrelation function (8) on the ideal geometry. Values of mean offset of 0.5 nm and a correlation length of 5 nm are chosen. Since the variations are imposed independently on each wall, the local change of the diameter can reach 1 nm. Fig. 4 compares densities of the ideal and the rough wire.

Here we again invoke as a reference the classical electron density, which follows the pattern of the walls, since the latter rigidly reflect the impinging electrons. In the quantum case the density smoothly follows the change in shape of the wire: The scale of local potential and thus of classical density variations differs from the scale of the quantum density variations. The latter appears as a distance quantity averaged over a few nanometers. This provides a strong argument in favor of the mode space approach which may be applied piecewise on the same scale.

The electron path in the rough wire is longer as compared to the ideal case, which should be reflected by a reduction of the current.

This is indeed the case in Fig. 5, showing the current evolution in the ideal and rough wires for three different values of k_{0y} of the injected states, corresponding to kinetic energies of 100 meV, 50 meV, and 25 meV. It is seen that states with lower kinetic energy need more time to establish stationary conditions. Furthermore, the effect of the roughness on such states is more pronounced, giving rise to a higher reduction of the current.

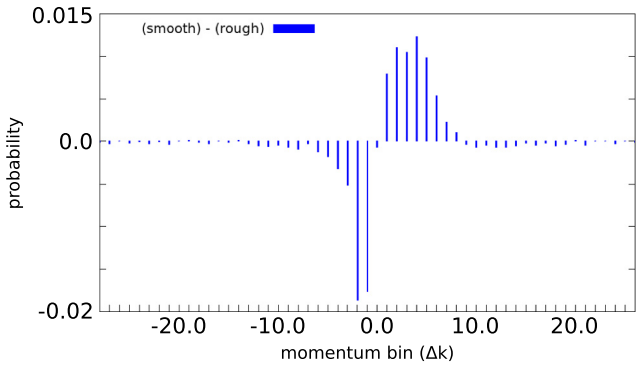

Fig. 6. Difference of the ideal and rough marginal **k** distributions in transport direction.

These current evolution simulations provide practical information about the relevance of the stochastic model of Section 2 for surface roughness aware transient approaches. As discussed, the first assumption requires sufficient time for establishing the energy conserving delta function. As seen from Fig. 5, the transient time until the establishment of the stationary current in the simulated structure and injected electrons with kinetic energy at and above the equilibrium energy $kT = 25$ meV is in the range of 100–200 fs. For a typical semiconductor the time for establishing the energy conserving delta function is less, but of this order [9]. For faster transitions any stochastic model based on the Fermi Golden Rule must be replaced by a non-Markovian approach [28].

Useful information is provided by the comparison of the k_y distribution (which is proportional to the y-component of the electron velocity $\hbar k_y/m$) in the rough and in the ideal wires.

Fig. 6 shows a histogram of the difference between the ideal and the rough marginal k_y distributions. Here again the ideal case serves as reference picture. Since there is no reflection in the transport direction, all velocities point in the positive direction. The difference of the wave vector probability distributions shows both a reduction of the probability for high values and the existence of negative values due to the quantum reflection caused by the rough potential.

5. Computational aspects

The simulations discussed in this work have been generated by using the free open source Wigner Ensemble Monte Carlo (WEMC) simulator shipped with ViennaWD.[1] WEMC is a C-based simulator controlled by a Lua script frontend for simulator control, supporting quantum transport simulations of one- and two-dimensional nanoelectronic structures. The simulator solves the semi-discrete Wigner equation, using the signed particle MC approach. Access to a development repository is available upon request. The tool supports single and continuous injection of minimum uncertainty wave packets as well as arbitrary shapes of potential barriers and other various parameters. The simulator offers parallel execution in a distributed-memory environment based on the message passing interface and a domain decomposition approach.

The simulations were performed on VSC-3[2] which represents the currently largest supercomputer in Austria. The system consists of 2020 nodes, each equipped with 2 Intel Xeon E5-2650v2 (total of 16 physical and 32 logical processors per node) and 64 GB of main memory. The network is based on a fat tree topology powered by an Intel QDR-80 dual-link InfiniBand fabric.

[1] http://viennawd.sourceforge.net/.
[2] http://vsc.ac.at/systems/.

6. Conclusions

Wigner signed particles provide both a comprehensive and intuitive computational approach for analyzing the physical effects induced by surface roughness in quantum wires. The major effects are caused by a combination of the fluctuation in the surface potential caused by the rough surface, and the quantum repulsion from the potential walls. This is in contrast with the classical behavior, and thus explains the failure of surface roughness models which rely on a classical picture where particles interact with the wall, to adequately describe the electron transport in quantum wires. Advanced models, such as the one derived in this work, correctly account for this phenomena via solutions of the Schrödinger equation in the confined direction. Such models rely on approximations like the mode space approach and statistical averaging to avoid the problem of having to simulate a statistical ensemble to gain a meaningful average.

From a classical point of view these approximations conflict with the existence of surface roughness. However, the behavior of the quantum density supports their application: In a numerical treatment the wire is decomposed into slices considered as homogeneous. In general, the physical conditions along the wire must vary smoothly in order to both, allow the statistical treatment of the surface imperfections and to avoid contact effects, which may be caused, e.g., by highly nonequilibrium conditions along the wire.

Based on the presented simulations we analyze the physical aspects of the electron transport in rough quantum wires. However, we have also shown that signed particle algorithms provide a rigorous and convenient approach for analyzing a variety of engineering problems related to confined electron transport.

Acknowledgments

We are grateful to Dr. Ewan Towie for the valuable discussions and suggestions regarding the surface roughness scattering model. The financial support by the Austrian Science Fund (FWF) project FWF-P29406-N30, the EC SUPERAID7 project 688101, the Austrian Federal Ministry of Science, Research and Economy, the National Foundation for Research, Technology and Development, and the Bulgarian Science Fund project DN-12/5 is gratefully acknowledged. The computational results presented have been achieved using the Vienna Scientific Cluster (VSC).

References

[1] P. Ellinghaus, J. Weinbub, M. Nedjalkov, S. Selberherr, Phys. Status Solidi R 11 (2017) 1700102-1–1700102-5. http://dx.doi.org/10.1002/pssr.201700102.
[2] S. Jin, M.V. Fischetti, T.-W. Tang, J. Appl. Phys. 102 (2007) 083715-1–083715-14. http://dx.doi.org/10.1063/1.2802586.
[3] C. Riddet, C. Alexander, A. Brown, S. Roy, A. Asenov, IEEE Trans. Electron Dev. 58 (2011) 600–608. http://dx.doi.org/10.1109/TED.2010.2095422.
[4] E.B. Ramayya, D. Vasileska, S.M. Goodnick, I. Knezevic, J. Appl. Phys. 104 (2008) 063711–1–063711–13. http://dx.doi.org/10.1063/1.2977758.
[5] E. Marin, (Doctoral thesis), Universidad de Granada, 2014 http://hdl.handle.net/10481/34203.
[6] E. Wigner, Phys. Rev. 40 (1932) 749–759. http://dx.doi.org/10.1103/PhysRev.40.749.
[7] M. Nedjalkov, R. Kosik, H. Kosina, S. Selberherr, Proceedings of the 7th International Conference on Simulation of Semiconductor Processes and Devices, SISPAD, 2002, pp. 187–190 http://dx.doi.org/10.1109/SISPAD.2002.1034548.
[8] M. Nedjalkov, H. Kosina, S. Selberherr, Microelectr. J. 34 (2003) 443–445. http://dx.doi.org/10.1016/S0026-2692(03)00069-7.
[9] M. Nedjalkov, D. Querlioz, P. Dollfus, H. Kosina, Nano-Electronic Devices: Semiclassical and Quantum Transport Modeling, Springer, 2011, pp. 289–358. http://dx.doi.org/10.1007/978-1-4419-8840-9_5.
[10] M. Nedjalkov, P. Schwaha, S. Selberherr, J.M. Sellier, D. Vasileska, Appl. Phys. Lett. 102 (2013) 163113-1–163113-4. http://dx.doi.org/10.1063/1.4802931.
[11] M. Nedjalkov, D. Vasileska, D.K. Ferry, C. Jacoboni, Ch. Ringhofer, I. Dimov, V. Palankovski, Phys. Rev. B 74 (2006). http://dx.doi.org/10.1103/PhysRevB.74.035311. 035311–035311.
[12] S. Goodnick, D.K. Ferry, C.W. Wilmsen, Z. Liliental, D. Fathy, O.L. Krivanek, Phys. Rev. B 32 (1985) 8171–8186. http://dx.doi.org/10.1103/PhysRevB.32.8171.
[13] J.M. Sellier, J. Comput. Phys. 297 (2015) 254–265. http://dx.doi.org/10.1016/j.jcp.2015.05.036.
[14] J.M. Sellier, I. Dimov, J. Comput. Phys. 280 (2014) 287–294. http://dx.doi.org/10.1016/j.jcp.2014.09.026.
[15] J.M. Sellier, I. Dimov, J. Comput. Phys. 270 (2014) 265–277. http://dx.doi.org/10.1016/j.jcp.2014.03.065.
[16] P. Vitanov, M. Nedjalkov, C. Jacoboni, F. Rossi, A. Abramo, Advances in Parallel Algorithms, IOS Press, 1994, pp. 117–128.
[17] M. Nedjalkov, H. Kosina, S. Selberherr, C. Ringhofer, D. Ferry, Phys. Rev. B 70 (2004) 115319-1–115319-16. http://dx.doi.org/10.1103/PhysRevB.70.115319.
[18] I. Dimov, World Scientific, 2008 http://dx.doi.org/10.1142/9789812779892.
[19] I. Dimov, M. Nedjalkov, J.M. Sellier, S. Selberherr, J. Comput. Electron. 14 (2015) 859–863. http://dx.doi.org/10.1007/s10825-015-0720-2.
[20] M. Nedjalkov, D. Vasileska, I. Dimov, G. Arsov, Monte Carlo Methods Appl. 13 (2007) 299–331. http://dx.doi.org/10.1515/MCMA.2007.017.
[21] H. Kosina, M. Nedjalkov, S. Selberherr, J. Appl. Phys. 93 (2003) 3553–3563. http://dx.doi.org/10.1063/1.1544654.
[22] H. Kosina, M. Nedjalkov, S. Selberherr, Monte Carlo Methods Appl. 10 (2004) 359–368. http://dx.doi.org/10.1515/mcma.2004.10.3-4.359.
[23] M. Nedjalkov, D. Vasileska, J. Comput. Electron. 7 (2008) 222–225. http://dx.doi.org/10.1007/s10825-008-0197-3.
[24] I. Knezevic, Phys. Rev. B 77 (2008) 125301-1–125301-18. http://dx.doi.org/10.1103/PhysRevB.77.125301.
[25] P. Ellinghaus, (Doctoral thesis), TU Wien, 2016 http://www.iue.tuwien.ac.at/phd/ellinghaus/.
[26] M. Nedjalkov, S. Selberherr, D.K. Ferry, D. Vasileska, P. Dollfus, D. Querlioz, I. Dimov, P. Schwaha, Ann. Phys. 328 (2012) 220–237. http://dx.doi.org/10.1016/j.aop.2012.10.001.
[27] H. Kim, H. Min, T. Tang, J. Park, Solid State Electron. 34 (1991) 1251–1253. http://dx.doi.org/10.1016/0038-1101(91)90065-7.
[28] B. Novakovic, I. Knezevic, Fortschr. Phys. 61 (2013) 323–331. http://dx.doi.org/10.1002/prop.201200071.